# Charging properties of gold clusters in different environments

Alexander Held,[1] Michael Moseler,[2] and Michael Walter[1]
[1]*Freiburg Materials Research Center, Stefan-Meier-Str. 21, 79104 Freiburg, Germany*
[2]*Fraunhofer Institute for Mechanics of Materials IWM, Wöhlerstrasse 11, 79108 Freiburg, Germany*
(Received 30 October 2012; published 10 January 2013)

The charge-dependent capacitance of gold clusters in the gas phase, protected by ligands and stabilized in ionic liquids, is investigated using density functional theory. For strong compounds such as naked or monolayer protected clusters, structural relaxation due to charging is effective only for very small species. The charge-dependent capacitance is mainly governed by two distinct electronic factors: the change in the effective charge centroid and the strong influence of electronic shell closings of the delocalized electrons. Both effects can be found and explained from within a simple jellium model. In contrast, soft compounds between gold clusters and ionic liquids undergo a structural reorganization during the charging process which results in a pronounced peak in the capacitance at zero charge.

DOI: 10.1103/PhysRevB.87.045411 PACS number(s): 63.22.Kn, 73.22.−f, 71.15.Mb

## I. INTRODUCTION

Transition-metal nanoparticles (TMNPs) are considered promising stable building blocks for future electronic devices,[1] nanocatalysts,[2–4] and medical marker applications.[5] TMNPs can be stabilized by different environments, such as dendrimers,[6] polymers,[1] DNA,[7] and even in ionic liquids.[8] Presumably, the best known TMNPs are currently clusters and nanoparticles formed by gold.[5] The fact that gold nanoparticles can be produced experimentally in wet chemical synthesis with atomic precision as well as their excellent stability renders these nanosystems interesting components in nanoelectronic devices such as single-electron transistors.[9]

Currently, the most studied and best characterized gold clusters are monolayer protected with ligands that are covalently bound to the metallic core forming a strong protecting layer. In particular, for thiolate protected gold clusters, a steadily increasing number of structures are discovered[10] deriving their stability by special electronic[11,12] and structural properties.[13,14]

One powerful experimental technique to characterize the electronic structure of TMNPs is cyclovoltammetry. With this method, the stability of thiol protected clusters for more than 10 different charge states has been demonstrated.[15] Similarly, thiol protected gold nanoparticles with 1.7-nm mean diameter in ionic liquid (IL) environment have been observed to provide up to 16 different charge states that were assigned to $-6 \leqslant z \leqslant +9$.[16] These systems are usually investigated in electrolyte solution, where a minimal capacitance at charge $z = 0$ is found, a finding that can be explained by classical Poisson-Boltzmann models.[15,17]

Recently, it has been discovered that also "ligand-free" gold clusters in ionic liquids (IL) show quantized charging.[18] In this experiment, a strong variation of the clusters capacitance for different charge states was detected. Interestingly, the maximum capacitance was recorded for the neutral cluster, in sharp contrast to the gold clusters in conventional electrolytes. An *ab initio* density functional theory (DFT) model explained this effect by a structural reorganization of the IL ion pairs surrounding the cluster.[18]

The literature on *ab initio* calculations of metal clusters at high-charge states and the effect on their capacitance is rather scarce.[19,20] Here, we investigate the behavior of gold clusters in different environments depending on their charge state. We address the charging properties of metal clusters under the influence of their environment in a wide range of charge states by *ab initio* calculations.

The paper is organized as follows. After a description of the computational methods (Sec. II), we consider the general framework to describe the charging of nanoscale objects and compare simple jellium models with our more realistic *ab initio* models of gas-phase gold clusters (Sec. III). The same strategy is applied to ligand protected gold clusters (Sec. IV) and gold clusters stabilized in ionic liquids (Sec. V). For the latter, a simple extended jellium model is introduced that agrees amazingly well with the *ab initio* results for charging of Au clusters immersed in IL.

## II. METHODS

We use density functional theory[21,22] to describe the electronic system and its interaction with the ionic configuration. The Kohn-Sham states and the electron density are represented within the projector augmented wave method[23] on real-space grids.[24,25] A 0.2 Å grid spacing was used for the representation of the smooth wave functions and we have carefully checked this choice for convergence. The exchange-correlation energy was approximated taking into account the gradient corrections (GGA) proposed by Perdew, Burke, and Ernzerhof (PBE).[26] First studies of gold-IL interactions showed that the application of the next higher level approximation [meta-GGA (Ref. 27)] gave no qualitative changes.[28,29] The structures were considered to be relaxed when the forces fell below 0.05 eV/Å.

## III. CHARGING OF GAS-PHASE CLUSTERS

In order to understand the capacitive properties of stabilized metal clusters, it is useful to study the behavior of the clusters under charging conditions in the gas phase first. There are a few *ab initio* studies in the literature about charging behavior of pure metal clusters. Weigend *et al.* studied a fictitious $Au_{309}$ cluster with DFT and found small structural relaxations due to charging.[19] Reimers and Hush studied the capacitance of gold clusters in the INDO/S approximation and found deviations from the classical electrostatic behavior.[30] A

 

tight-binding model applied by Senet and Hou leads to the expected capacitance $C \propto n^{1/3}$ behavior for $Cu_n$ clusters,[31] whereby $Ba_n$ clusters were found to show more complicated dependence on the number of atoms $n$ (Wang *et al.*[20]). Recently, Batista and coworkers studied ionization potentials and electron affinities of bare and protected gold clusters as a function of their size.[32]

Generally, the energy of a nanoscale system $E$ depending on the number of additional electrons $N$ can be expressed as[33]

$$E(N) = E_0 - \chi N + \eta N^2 + \ldots, \tag{1}$$

where $E_0$ is the energy of the neutral system, $\chi$ the absolute electronegativity, and $\eta$ the absolute hardness of the system.[34] The dots indicate possible higher-order contributions in $N$. Writing Eq. (1) in terms of the charge state $z = -N$, one arrives at

$$E(z) = E_0 + \chi z + \frac{z^2 \mathrm{e}^2}{2C} + \ldots, \tag{2}$$

where e is the unit charge and we have identified $\mathrm{e}^2/(2\eta)$ with the system capacitance $C$. In a classical capacitor $\chi = 0, \eta > 0$ and all higher-order terms vanish. Small systems often provide a positive electron affinity $A = \chi - \eta > 0$ and generally their ionization potential is larger than the electron affinity ($I > |A|$) which results in a positive $\chi = (I + A)/2$. To minimize surface energy, metal clusters usually are found in a more or less round shape, which suggests the comparison to a classical metal sphere. The sphere radius is not well defined at the atomic scale, but can be obtained through the capacitance

$$C = 4\pi\epsilon_0 r_{\mathrm{eff}} \tag{3}$$

as the systems' effective radius $r_{\mathrm{eff}}$.

Already in the mid 1980s Perdew applied a jellium model for monovalent metal clusters. Within this model, the effective radius has been predicted as[35]

$$r_{\mathrm{jell}} = r_s N^{\frac{1}{3}} + a(r_s) \tag{4}$$

with the Wigner-Seitz radius $r_s = (3/4\pi n)^{1/3}$ obtained from the electron density $n$ in the bulk. The electronic spill-out factor $a(r_s)$ depends on $r_s$ and is found to be nearly independent of the cluster size $N$. Later on, a liquid drop model within the stabilized jellium model[36,37] has been presented that also describes the size dependence of the absolute electronegativity $\chi$.

There has been much progress in the understanding of electronic and structural properties of metal clusters in the last decades. In particular, density functional theory has been successful in describing and exploring these systems. Less attention has been paid in the literature to the validity of Eq. (2) for charge states higher than $z = -1,0,1$, which are well possible for metal clusters. We will investigate the clusters at higher charge states where we will in particular concentrate on the charge-dependent capacitance. We will see that this quantity gives a very meaningful and sensitive measure of the clusters' charging properties. The charge-dependent capacitance can be obtained from the energy using Eq. (2) via the finite-difference expression

$$C_{\mathrm{fd}}(z) = \frac{\mathrm{e}^2}{E(z+1) - 2E(z) + E(z-1)}, \tag{5}$$

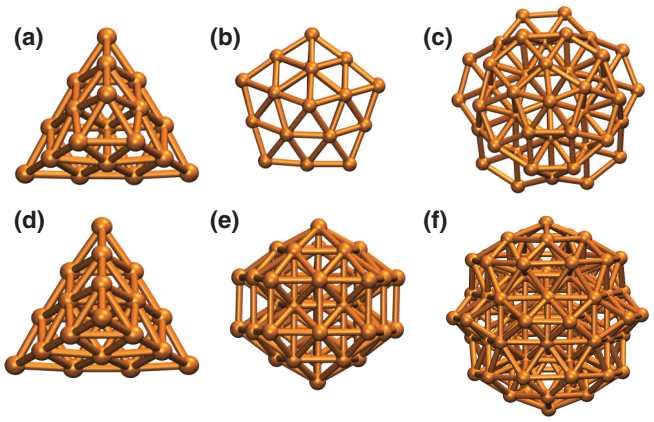


FIG. 1. (Color online) Structures of (a) $Au_{19}$, (b) $Au_{39}$ top view, (c) $Au_{79}$ top view, (d) $Au_{20}$, (e) $Au_{39}$ side view, and (f) $Au_{79}$ side view.

where the quantized nature of the charge is implicitly taken into account.

We study gold clusters in four sizes as depicted in their neutral ground-state configuration in Fig. 1. The two smaller tetrahedral clusters $Au_{19}$ and $Au_{20}$ are known to be stable ground-state isomers in the gas phase.[38,39] These clusters are very symmetric and are known to show strong shell effects. We also consider two larger model structures $Au_{39}$ and $Au_{79}$ that were obtained from the experimental crystal structure of $Au_{102}(SR)_{44}$ (Refs. 11 and 40) by removing the outer layers. The configurational ground-state structures of $Au_{39}$ and $Au_{79}$ clusters are unknown up to date.

In order to judge the accuracy of the PBE approximation for gold, we calculated the ionization potential $I_1 = 9.54$ eV and the electron affinity $A_1 = 2.31$ eV of a single gold atom. $I_1$ and $A_1$ are in good agreement with the experimental values $I_1^{\mathrm{exp}} = (9.22553 \pm 0.00002)$ eV (Ref. 42) and $A_1^{\mathrm{exp}} = (2.3086 \pm 0.0007)$ eV.[43] Also, our PBE values $A_{19} = 3.58$ eV and $A_{20} = 2.77$ eV for the adiabatic electron affinities of $Au_{19}$ and $Au_{20}$ are in good agreement with the experimental values $A_{19}^{\mathrm{exp}} = (3.610 \pm 0.050)$ eV (Ref. 43) and $A_{20}^{\mathrm{exp}} = (2.745 \pm 0.015)$ eV.[38] The PBE values for the vertical ionization potential $I_{19} = 6.63$ eV and $I_{20} = 6.98$ eV underestimate the experimental values[44] of $I_{19}^{\mathrm{exp}} = 7.70$ eV and $I_{20}^{\mathrm{exp}} = 7.82$ eV.

In Table I, we compare our results for the ionization potentials and electron affinities to previous calculations for different cluster sizes. For the adiabatic values, all structures have been allowed to relax in their charge states, whereas for the vertical values the structure was fixed at the neutral ground-state structure. Our values are in good agreement with those of Batista *et al.*[32] where the PBE functional was also used. There is even agreement for $Au_{79}$, although a truncated octahedral symmetry has been used for this cluster in their study. Assadollahzadeh and Schwerdtfeger[41] used the hybrid B3PW91 functional. The two functionals agree well with regard to the changes between the different cluster sizes, however, the electron affinities are lower within the B3PW91 functional. Table I also lists the finite-difference capacitance $C_{\mathrm{fd}}$ for the neutral clusters. As can be expected, $C_{\mathrm{fd}}$ increases monotonously with the cluster size. $Au_{20}$ represents an exception, where the capacitance drops off significantly.

TABLE I. PBE results for the ionization potentials $I$ and electron affinities $A$ of gold clusters in the gas phase with derived values for the capacitance $C = C_{\rm fd}(z = 0)$. Energies are given in eV, capacitance in zF $= 10^{-21}$ F.

| | $I$ | | $A$ | | $C$ |
|---|---|---|---|---|---|
| $Au_1$ | 9.54 9.35[a] 9.54[b] | | 2.31 2.09[a] | | 22.1 |
| | Adiabatic | Vertical | Adiabatic | Vertical | Adiabatic |
| $Au_{19}$ | 6.57 | 6.63 6.46[a] | 3.58 | 3.52 3.42[a] | 53.5 |
| $Au_{20}$ | 6.97 | 6.98 7.22[a] | 2.77 | 2.72 2.38[a] | 38.2 |
| $Au_{39}$ | 5.85 | 5.86 | 3.40 | 3.41 | 65.4 |
| $Au_{79}$ | 6.00 | 5.95 5.89[bc] | 4.05 | 4.00 3.93[bc] | 82.4 |

[a]Reference 41.
[b]Reference 32.
[c]Truncated octahedral symmetry.

This effect can be explained by an electronic shell closing as we will find in the end of this section.

In a next step, we want to study the behavior of $C_{\rm fd}(z)$ for $z \neq 0$. The smaller $Au_{19}$, $Au_{20}$, and $Au_{39}$ take their energetic minimum at $z_{\rm min} = -2$, and for $Au_{79}$ the energy is minimal at $z_{\rm min} = -3$. Charge states $z < z_{\rm min}$ are unstable against the removal of the extra electrons. For these unstable states, our calculations still converge with all excess electrons located near the cluster surface due to the finite size of the box. Interestingly, even in this unphysical situation, the energy is still reasonable which is why we allowed to include some of these charge states to our analysis. Note also that in the region of positive charge, we have used rather large charges up to $z = 6$, more than can be expected to be stable on clusters of this small size.[45] For example, $Au_{20}$ is energetically unstable against the transition

$$Au_{20}^{z} \rightarrow Au_{19}^{z-1} + Au^{+}$$

for $z > 2$. Such fission events are hindered by rather high barriers, however.[46] Indeed, some of the highly charged clusters (e.g., $Au_{20}^{8+}$) fragmented during the relaxation process and these were excluded from our study.

The resulting charge-dependent capacitance $C_{\rm fd}$ is shown in Fig. 2 for both relaxed and unrelaxed structures (i.e., structures fixed at neutral geometry). Notably, no significant influence of the structural relaxation to the capacitance could be found within the observed charge range. There are some sudden jumps of the capacitance that arise from electronic shell effects discussed later in this section. Apart from this, all investigated clusters show a rising capacitance for increasing number of excess electrons. This brings us to the question as to where the excess charge goes to or is depleted from when the charge state of the cluster is changed. We can define the radial excess electron density $\Delta n_r^-$ and the radial excess hole density $\Delta n_r^+$ as

$$\Delta n_r^{\pm}(r,z) = \pm n_r(r,z) \mp n_r(r,z \pm 1), \qquad (6)$$

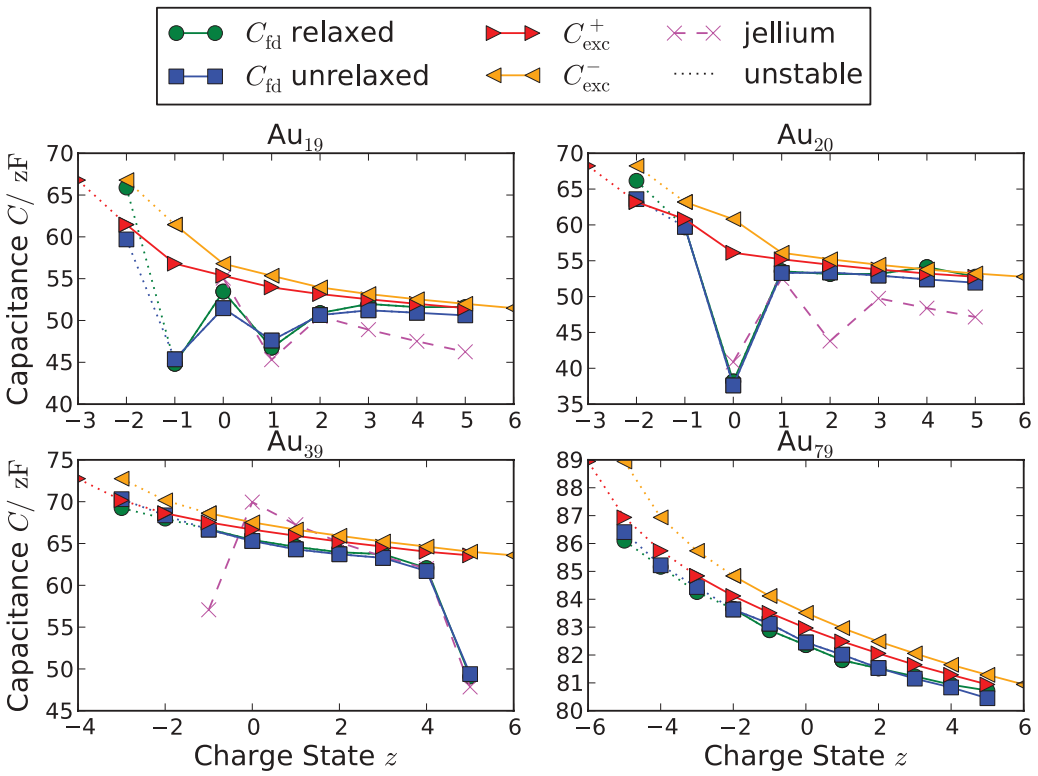


FIG. 2. (Color online) The charge-dependent capacitance for the $Au_N$ clusters ($N = 19,20,39,79$) in the gas phase. The finite-difference capacitance $C_{\rm fd}$ obtained from PBE energies and the capacitance from the jellium calculation include shell effects. The capacitance $C^{\pm}_{\rm exc}$ calculated from the radial excess charge centroid [Eq. (9)] captures the shrinking of the electron cloud with increasing positive excess charge (1 zF $= 10^{-21}$ F).

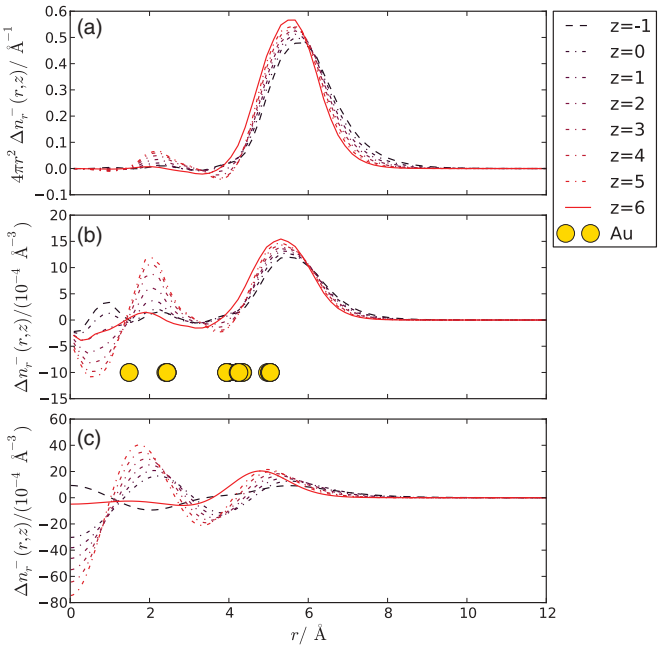


FIG. 3. (Color online) (a) The radial excess charge distribution $4\pi r^2 \Delta n_r^-$ and (b) the radial excess electron density $\Delta n_r^-$ for the $Au_{39}$ cluster in the gas phase from the full DFT calculation. (c) The radial excess electron density of the corresponding spherical jellium model with a square potential.

where $n_r$ is the radial electron density

$$n_r(r,z) = \frac{1}{4\pi} \int_{\phi=0}^{2\pi} \int_{\theta=0}^{\pi} n[\vec{r}(r,\phi,\theta),z] \sin\theta \, d\theta \, d\phi \ , \quad (7)$$

i.e., the charge-dependent electron density $n(\vec{r},z)$ averaged over azimuthal and polar angles $\theta$ and $\phi$, respectively. Here, $r$ is defined by the distance from the center of mass of the cluster. $\Delta n_r^-(r,z)$ is the density of the extra electron when the electron number is increased and $\Delta n^+(r,z)$ is the density of the missing electron when the electron number is decreased, therefore, $\Delta n_r^-(r,z) = \Delta n^+(r,z-1)$ holds.

The radial excess electron distribution is shown in Fig. 3(a) for the $Au_{39}$ cluster as an example where the atom positions are fixed at the configuration of the neutral cluster. The figure shows that the $Au_{39}$ cluster mainly behaves like a small metal sphere: nearly all of the excess charge is concentrated on the surface of the cluster. In contrast to a classical metal sphere, the peak position of $n_r(r,z)$ depends slightly on the charge state and there is polarization of the cluster interior that increases with increasing positive charge. The polarization effect is more appreciable when the excess charge density is plotted as shown in Fig. 3(b).

The excess charge distribution is very similar to the radial charge densities shown by Batista *et al.*[32] These authors interpreted the large variation of the charge density change inside the cluster as a sign of the metal to nonmetal transition. This topic is of renewed interest as it was shown recently that small sodium clusters retain their metallic behavior (defined by the screening of the electric dipole moment) up to the smallest sizes.[47,48] In order to shed light on the origin of the density variations inside the clusters, we compare the excess charge distribution from a jellium model using a square potential similar to the model used in Ref. 35. We have used $r_s = 1.59$ Å as appropriate for gold that results in a jellium ball of 5.4 Å radius to describe the $Au_{39}$ cluster. The electronic structure in this model is solved by DFT in the local density approximation.[49] Comparing Figs. 3(b) and 3(c) shows that the density variations are qualitatively very similar to the full calculation. Quantitatively, the jellium model shows even larger variations of $\Delta n_r^-$ inside the cluster, which would be a sign of a larger nonmetallic property in the jellium model in the interpretation adopted in Ref. 32. The density variations relative to the constant background are pure electron confinement effects due to the wave nature of the electrons, however. Clearly, these effects will diminish in the limit of large clusters, but are not in contradiction with metallicity.

Due to the variability of the excess charge with the charge state, a small gold cluster does not have a fixed radius. In order to analyze the effect of the excess charge locations to the capacitance, we define the radial excess charge centroid as the radial expectation value to

$$r_{\rm exc}^{\pm}(z) = 4\pi \int_0^{\infty} r^3 \ \Delta n_r^{\pm}(r,z) dr$$
$$= \int \|\vec{r}\| \Delta n^{\pm}(\vec{r},z) d^3r, \quad (8)$$

which would simply give the radius of a classical metal sphere. A similar approach is applied in Ref. 32, where the radius is defined through the last inflection point of the radially averaged electron density. The corresponding capacitance is

$$C_{\rm exc}^{\pm}(z) = 4\pi\varepsilon_0 r_{\rm exc}^{\pm}(z), \quad (9)$$

which is depicted also in Fig. 2. The decrease of $r_{\rm exc}^{\pm}(z)$ with increasing positive charge describes the smooth decrease of the capacitance $C_{\rm fd}$ very well. Thus, the main effect here is the shrinking of the electron cloud with increasing positive cluster charge.

Figure 4 compares the radii obtained from the different methods for all the clusters considered. The $r_{\rm exc}^{\pm}$ are contrasted to the finite-difference radius $r_{\rm fd} = C_{\rm fd}/(4\pi\varepsilon_0)$ and to the

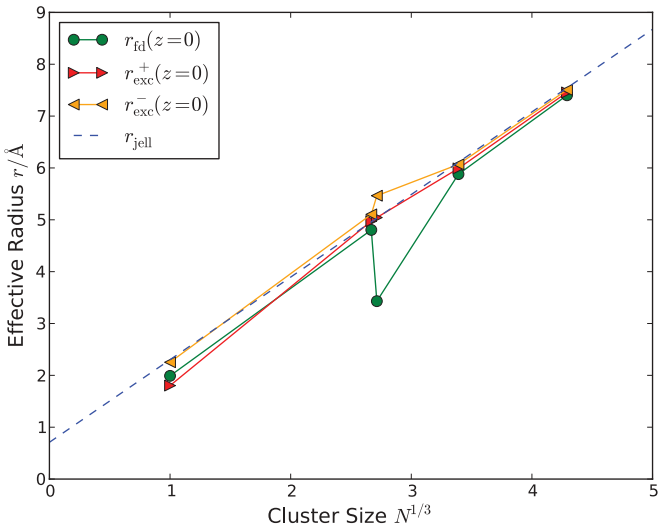


FIG. 4. (Color online) Radial excess charge centroid $r_{\rm exc}^{\pm}(z=0)$ and finite-difference radius $r_{\rm fd}(z=0)$ as a function of the cube root of the cluster size $N$ compared to the jellium model of Eq. (4).

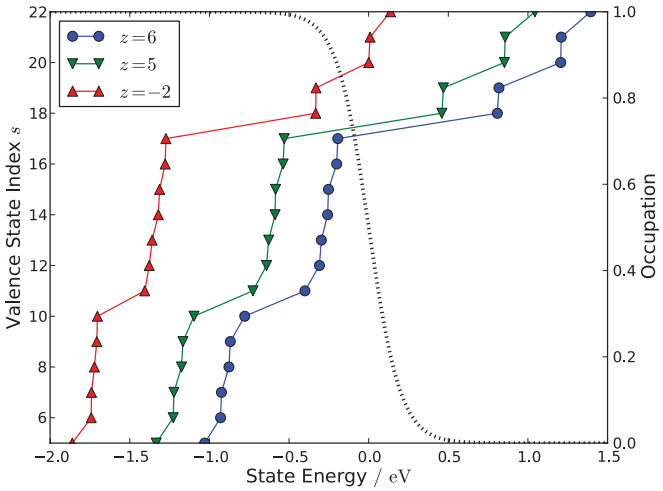


FIG. 5. (Color online) The distribution of Kohn-Sham states relative to the Fermi level for different charge states of $Au_{39}$. The plot also shows the states' occupancy due to the finite Fermi width of 0.1 eV used in our calculations.

predictions from the jellium model of Eq. (4). For the latter, we have used the values $r_s = 1.59$ Å, $a(r_s) = 0.71$ Å for gold, as given by Perdew.[35] By plotting the radii as a function of the cube root of the cluster size $N$, the jellium model results in a straight line. The computed radii are generally in good agreement with the jellium prediction showing again the applicability of this simple model for gold clusters. The exception is $r_{\mathrm{fd}}$ of $Au_{20}$, where a shell closing occurs at $z = 0$.

The analysis of the effect of shell closings is again exemplified for $Au_{39}$. In this cluster, a rather large deviation is found between the prediction of the charge centroid and $C_{\mathrm{fd}}(z)$ for $z = 5$ in Fig. 2. This is the manifestation of an electronic shell closing. To see this, we plot the density of the Kohn-Sham states for three different charge states in Fig. 5. The $s$-valence-state index was obtained by counting relative to the 195 doubly occupied $d$-derived valence states in the total valence-state count.[50] The structure of the density of states is very rigid under the change of the charge state. The latter results merely in a shift of the Fermi energy. Exactly for $z = 5$, there are 34 $s$-derived electrons in the cluster. 34 electrons represent a strong magic number, where the spherical jellium $1f$ shell[51] is closed. In accordance with this picture, there is a block of seven states below the $z = 5$ Fermi level that corresponds to the $1f$ shell. A decomposition of the Kohn-Sham states into spherical harmonics relative to the cluster's center[11] (not shown) is in line with this assignment. It is the same shell closing that is responsible for the stability of the well-known $[Au_{39}Cl_6(PR_3)_{14}]^{-1}$ cluster,[11,52,53] which is of different structure and will be analyzed in the following section. In the gas-phase $Au_{39}$ cluster, this shell closing manifests itself as a large gap of about 1 eV. Beginning at the charge $z = 6$, the jellium $1f$ shell below this gap is starting to get depleted. According to the finite-difference definition (5), $C_{\mathrm{fd}}(z = 5)$ involves the energy at $z = 6$ and hence is affected by this step that leads to the observed sudden decrease in the capacitance (cf. Fig. 2).

According to the jellium model, the closing of the $2p$ shell at $z = -1$ where there are 40 $s$-derived electrons in the cluster also leads to a significant drop of the capacitance of $Au_{39}$ as can be seen in Fig. 2. However, there is no such drop for the PBE calculation. This is because the $2p$ states are not degenerate anymore in the nonspherical geometry of the $Au_{39}$ cluster. Indeed, the decomposition of the Kohn-Sham states into spherical harmonics reveals that the block of seven $1f$ states is followed by two (doubly occupied) states with only 50% $p$ symmetry and by two states with 86% $g$ symmetry, whereas in the jellium model, the occupation order starting from the block of seven $1f$ states is $1f^{14}2p^{6}1g^{18}$ with a gap between the $2p$ and $1g$ states.[51]

The jellium model nicely explains also the sudden variation of $C_{\mathrm{fd}}$ for the other clusters shown in Fig. 2. In the case of $Au_{19}$, both the jellium $1d$ and $2s$ shell closings at $z = -1$ and $+1$ are present in the PBE calculation. The jellium capacitance at $z = -1$ is not shown in Fig. 2 since $z = -2$ is not a stable configuration for $Au_{19}$ in the jellium model. For $Au_{20}$, the situation is different: only the $2s$ shell closing at $z = 0$ is visible in the PBE calculation, while the gap at $z = +2$ is missing due to the strong tetrahedral symmetry.[54] For $Au_{79}$, there are no shell closings to be expected from the jellium model in the observed charge range in accordance with our PBE calculation.

## IV. LIGAND PROTECTED CLUSTERS

We now turn to the case of monolayer protected clusters (MPCs). Here, we study the charge-dependent capacitance of three thiolate protected and of three phosphene/chlorine stabilized clusters. We chose three thiolate protected clusters that correspond to the experimentally completely characterized $Au_{25}(SR)_{18}$,[55,56] $Au_{38}(SR)_{24}$,[57] and $Au_{102}(SR)_{44}$.[40] The larger thiol groups SR in the experiment have been replaced by $SCH_3$ giving $Au_{25}(SCH_3)_{18}$,[58] $Au_{38}(SCH_3)_{24}$,[59,60] and $Au_{102}(SCH_3)_{44}$ (Ref. 11) in our simulations. For the phosphene/chlorine stabilized clusters, we chose the two structurally well-known $Au_{11}(PH_3)_7Cl_3$ (Refs. 11 and 61) and $Au_{39}(PH_3)_{14}Cl_6$.[52,53] These are extended by the lately proposed model for the "Schmid-gold" cluster of composition $Au_{69}(PH_3)_{20}Cl_{12}$ by two of us.[62]

The explicit cluster structures were taken as obtained from earlier studies, i.e., $Au_{25}(SCH_3)_{18}$ from Ref. 58, $Au_{38}(SCH_3)_{24}$ from Ref. 60, $Au_{102}(SCH_3)_{44}$ from Ref. 11, $Au_{11}(PH_3)_7Cl_3$ from Ref. 11, $Au_{39}(PH_3)_{14}Cl_6$ from Ref. 53, and $Au_{69}(PH_3)_{20}Cl_{12}$ from Ref. 62. All structures were relaxed in the charge state that leads to a large highest occupied molecular orbital and lowest unoccupied molecular orbital (HOMO-LUMO) gap (see below) and their structures are shown in Fig. 6.

Figure 7 summarizes the charge-dependent capacitance of all considered MPCs. Charging of the clusters at fixed nuclear configurations shows a rather flat $C(z)$ with a pronounced minimum at one specific charge state. It is the charge state where the large stabilizing HOMO-LUMO gap occurs, namely, at $z = 0$ for $Au_{11}(PH_3)_7Cl_3$, $Au_{38}(SCH_3)_{24}$, and $Au_{102}(SCH_3)_{44}$, and at $z = -1$ for $Au_{25}(SCH_3)_{18}$, $Au_{39}(PH_3)_{14}Cl_6$, and $Au_{69}(PH_3)_{20}Cl_{12}$. It is the same effect as we have already seen in the naked $Au_{39}$ cluster: the spherical [or cylindrical in case of the $Au_{38}(SCH_3)_{24}$][60] shell closing produces a remarkable minimum for otherwise rather constant $C(z)$. The

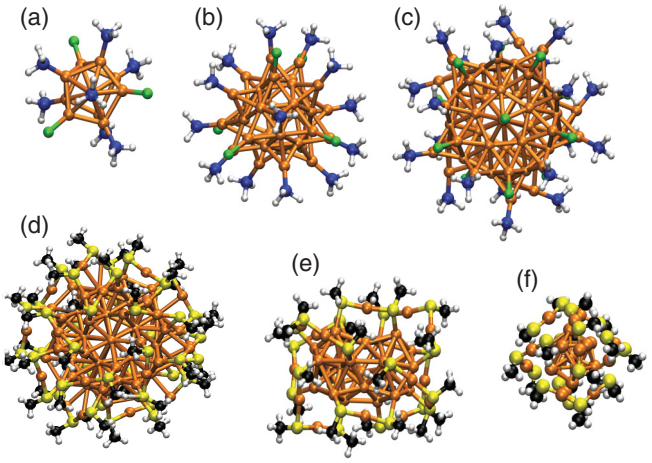


FIG. 6. (Color online) Structures of the ligand protected clusters considered: (a) $Au_{11}(PH_3)_7Cl_3$, (b) $Au_{39}(PH_3)_{14}Cl_6$, (c) $Au_{69}(PH_3)_{20}Cl_{12}$, (d) $Au_{102}(SCH_3)_{44}$, (e) $Au_{38}(SCH_3)_{24}$, and (f) $Au_{25}(SCH_3)_{18}$. Au: orange, P: blue, H: white, Cl: green, S: yellow, and C: black.

mean capacitance of the protected $Au_{39}(PH_3)_{14}Cl_6$ is slightly larger than that of the naked $Au_{39}$ cluster analyzed in the last section. This is a consequence of the more open structure of the protected species. For the smaller clusters $Au_{11}(PH_3)_7Cl_3$ and $Au_{25}(SCH_3)_{18}$, we have also tested the effect of structural relaxation. As shown in Fig. 7, this effect is relatively large for the small and open structure of the $Au_{11}(PH_3)_7Cl_3$. Already for the slightly larger and more compact $Au_{25}(SCH_3)_{18}$, the effect becomes marginal, very similar to the finding in the naked $Au_{39}$ cluster above. We therefore do not expect much of an effect due to structural relaxations for the larger clusters.

## V. GOLD CLUSTERS IN IONIC LIQUIDS

We finally turn our attention to the charging behavior of gold clusters stabilized in ionic liquids (ILs). A pronounced increase in capacitance around charge state $z = 0$ has been found recently for unprotected gold clusters in an IL.[18] This is in stark contrast to the case of MPCs in dilute electrolytes, where usually a capacitance decrease is observed for neutral clusters.[15]

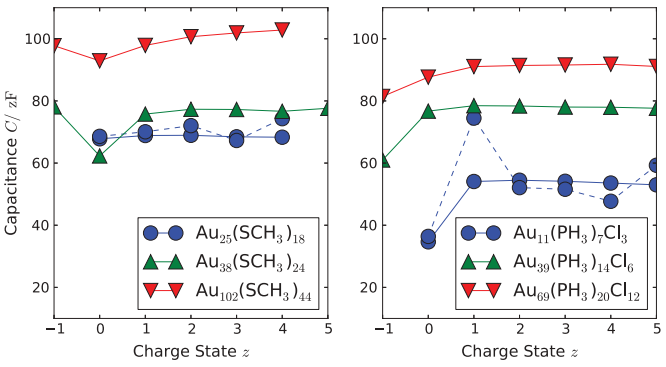


FIG. 7. (Color online) The charge-dependent capacitance of monolayer protected clusters (MPC). The capacitance obtained by clusters relaxed at each charge state is marked by a connecting dashed line.

The charging properties of metal nanoparticles (MNPs) in ionic liquids have not been modeled so far. There is extensive modeling of charged MPCs in electrolytes, however, where classical electrostatics is applied.[15,17,63] In these approaches, the Poisson-Boltzmann equation describing the electrolyte at a given temperature is solved in the presence of a protecting layer of defined static dielectric constant $\varepsilon$. In effect, this leads to a rise of the capacitance for increasing $z$ due to the formation of the electrolyte double layer. There exist extensions of this approach considering the penetration of the ions into the protecting layer with essentially the same result.[63]

Lately, it has become clear that the use of the Poisson-Boltzmann equation can become inadequate for ILs and the finite size of the ions has to be taken into account.[64] This can be done in a mean-field approach, by explicit molecular dynamics simulations of charged model particles[65] or by classical density functional theory.[66] However, these techniques have only been applied to planar metal electrodes and not to MPCs so far.

Compared to MPCs, not as much is definitely known about the actual stabilization mechanism and the structures present in the weak stabilization case of MNPs in ILs. Experimental studies indicate layered structure of ILs on metal electrodes that can change under variation of the electrode potential.[67] The layered structure might reach quite far into the IL bulk as ILs seem to provide mesoscopic structure even without the presence of charged electrodes.[68] The ion distribution around the MNP can be expected to form similar layered structure, where the finite size of the particle might play a significant role. This probably leads to a rather complicated and long-ranged structure around the MNP that is far out of scope of an *ab initio* simulation. Two of us have established a simple model for the cluster-IL interaction in Ref. 18, where only a limited number of IL ion pairs are taken into account. This model explains the experimental capacitance behavior very well. In the following, we will discuss this model in greater detail and contrast it with an electrostatic approach similar to Perdews' jellium model above.

Transmission electron microscopy investigations indicate that the smallest gold clusters that can be stabilized in ILs are of roughly 1.1 nm diameter,[18,28,29] which correspond to clusters of about 40 gold atoms. We therefore use the $Au_{39}$ model described and studied above also for the interaction with ILs as described below.

We model the clusters in contact with a varying number of IL ion pairs. The characterization of ILs by the properties of their ion pairs is a common practice.[69] In our case, this strategy helps to keep the IL environment neutral and to localize the total charge in the simulated system to the nanoparticle itself. We restrict ourselves to $BF_4$ BMIm (Ref. 70) ion pairs, which represent one of the most common IL and has also been used in the experiment.[18] The relaxed geometry of the isolated $BF_4$ BMIm pair is depicted in Fig. 8(a). We obtain a pairing energy of 3.36 eV in good agreement with the B3LYP result of 3.58 eV in a very similar configuration.[71] It was suggested that van der Waals corrections affect binding and structure of IL networks.[69,72] These effects are known to be poorly described by local and semilocal density approximations.[73] Application of a largely nonempirical van der Waals correction[74] increases the $BF_4$ BMIm pair binding energy slightly to 3.53 eV. We regard this change to be insignificant for a study of the charging

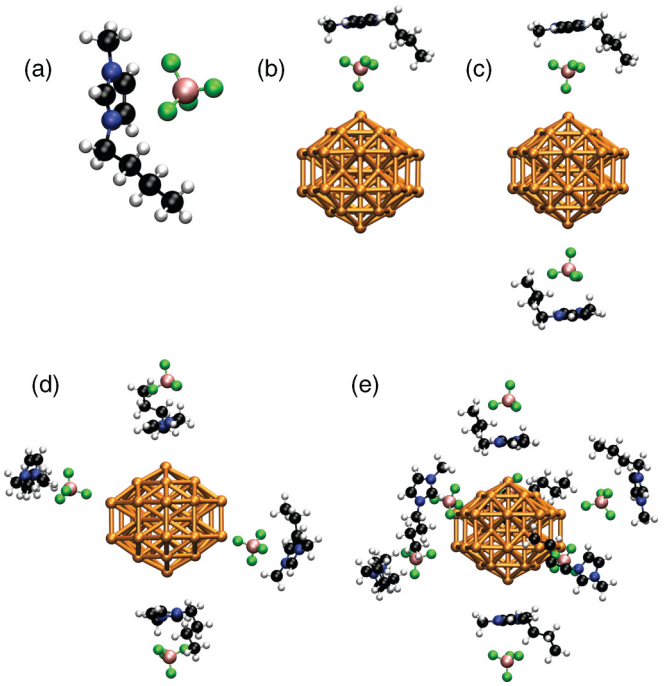


FIG. 8. (Color online) (a) Optimized structure of the $BMIm^+$ $BF_4^-$ pair. (b)–(d) Optimized structures of neutral $Au_{39}$ clusters in contact with 1, 2, 4, and 7 ion pairs. Au: orange, N: blue, H: white, F: green, B: pink and C: black.

properties and neglect van der Waals effects in the following. The main interaction between the ions is due to the strong Coulomb attraction. Assuming a positive unit charge located at the center of mass of the N atoms in $BMIm^+$ and a negative unit charge at the B atom of $BF_4^-$ in their equilibrium configuration, the electrostatic energy of this geometric dipole of length 3.77 Å would be 3.82 eV, therefore even a bit larger than the actual value, which is reduced due to the nonlocality of the electronic charge.[75]

Our model systems consist of the $Au_{39}$ cluster in contact with an increasing number of ion pairs $n_p = 1,2,4$, and 7. The ground-state structures of the neutral clusters are depicted in Fig. 8. As for the naked gas-phase clusters, we allow the configurations to relax to their local minimum without any symmetry restrictions.

A single-ion pair binds with 0.42 eV to the cluster in the configuration shown in Fig. 8(b). This is roughly half of the interaction energy of 1.0 eV between a $Pd_5$ cluster and $[MMIm][BF_4]$ pair obtained in a recent study.[76] Other ion-pair orientations relative to the cluster (not shown) are at least 0.24 eV higher in energy. The clear preference of this configuration can be explained by the strong binding between gold and anions.[28,29] Changing the clusters' charge $z$ can change the situation, however. For $z = -1$, the configuration where the cation points to the cluster is the lowest in energy, separated from other possible orientations by at least 0.2 eV. Now, the electrostatic energy overcomes the gold-anion binding. Orienting the pairs dipole parallel to the clusters' surface is always higher in energy and is hence not relevant here. We will therefore neglect this possibility in the following and allow the ion pairs to take one of two possible orientations, either pointing with the anion towards the cluster or with the cation only.

For configurations with more than one pair, we place the pairs in maximal separation on the cluster corners, where the clusters are most reactive. At each charge state $z$, we consider the possible perpendicular orientations of the pairs' dipoles relative to the cluster. Two pairs still bind preferably with $BF_4$ next to the neutral cluster, but the binding energy of the second ion pair is reduced to 0.26 eV. This trend continues and accordingly four pairs are found in a ground state of mixed configuration (see Fig. 8).

In order to give an easy characterization of the configurations depending on the clusters' charge $z$, we introduce the screening charge $z_2$ to be the sum of ionic charges nearest to the $Au_{39}$ cluster. This allows us to parametrize all investigated configurations of a fixed number $n_p$ of ion pairs attached to the gold cluster by only picking one representative configuration for each possible value of $z_2$. For example, Fig. 8(d) corresponds to the $(n_p = 4, z_2 = 0, z = 0)$ configuration, where half of the pairs point their anions and half of the pairs their cations towards the cluster.

We contrast the DFT results with an electrostatic model (EM) as depicted in Fig. 9. The charged cluster is modeled as a classical spherical capacitor with effective radius $r_1$ and the corresponding capacitance $C_1 = 4\pi\epsilon_0 r_1$. The IL ions are modeled as smeared-out charges $z_2$ and $-z_2$ at concentric spheres with radii $r_2$ and $r_3$, respectively, which form a capacitor

$$C_{23} = 4\pi\epsilon_0 \frac{r_2 r_3}{r_3 - r_2}. \tag{10}$$

The electrostatic energy of the entire model system is then given by

$$E(z_2,z) = \mathrm{e}^2 \left( \frac{z^2}{2C_1} + \frac{z z_2}{C_{23}} + \alpha \frac{z_2^2}{2C_{23}} \right), \tag{11}$$

if we require $E(z_2 = 0, z = 0) = 0$. We have neglected the effect of the absolute electronegativity $\chi$ at this point since it does not contribute to the capacitance. Note that a scaling factor $0 < \alpha \leqslant 1$ was introduced to the self-energy of the ionic system here, which captures effectively the discrete nature of the ionic charges. The discreteness leads to an overscreening effect not seen when completely smeared charges are assumed.[77] Generally, the scaling factor depends on the geometry as well as on the number of ion pairs, but we fix it to $\alpha = 0.24$ for simplicity in the following. This value

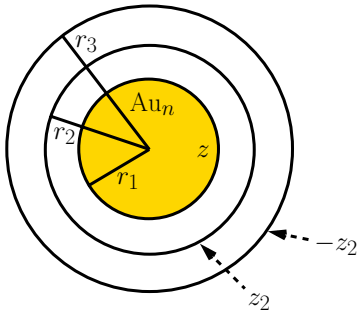


FIG. 9. (Color online) Electrostatic model for the interaction of a gold cluster and the surrounding ion pairs.

was obtained by a fit to the DFT results for $n_p = 4$, but can be obtained also from a comparison of the electrostatic energies of the smeared-out charge and the charge located at eight point charges resembling Fig. 8(d). The cluster radius is chosen to $r_1 = r_{\mathrm{fd}}(z = 0) = 5.88$ Å for $Au_{39}$. Using the distance of a $BMIm^+$ $BF_4^-$ ion pair and the average distance between the surface of the gold cluster and the nearest ions,[78] we obtain $r_2 = 9.58$ Å and $r_3 = 13.14$ Å.

For a fixed number of ion pairs $n_p$ and charge $z$, we search for the minimal energy configuration and define the corresponding energy to

$$E_{\min}(n_p,z) = \min_{z_2}\{E(n_p,z_2,z)\}. \tag{12}$$

This procedure can be applied both in DFT as well as in the EM, where in the latter case $n_p$ restricts the maximal possible $z_2$. In addition, we allow $z_2$ to adopt values that are possible in the DFT calculations only for the EM, i.e., $z_2$ is odd for odd $n_p$ and $z_2$ is even for even $n_p$. Figure 10 shows the minimizing $z_2$ for all configurations considered in our study. There is remarkable agreement between the EM and the DFT calculations. We discuss the EM results first and detail the differences in DFT afterwards.

For odd $n_p$, there are two degenerate minimal configurations $z_2 = \pm 1$ for the neutral cluster in the EM. Except, for $n_p = 7, z = \pm 1$, where $|z_2| = 5,7$ differ by only about thermal energy (taken to $k_B T = 26$ meV at $T = 300$ K), other $z_2$ values are well separated energetically from the minimum. Complete smearing out of the charges, i.e., $\alpha = 1$, would lead to $z_2 = -z$ for the minimizing configuration as can be seen from Eq. (11). The discreteness of the ion charges modeled using $\alpha = 0.24$ leads to an overscreening effect, where more charge is located on the spheres than on the cluster itself: For $n_p = 1,2,4$, all pairs are in the same direction relative to the clusters surface already at $|z| = 1$,

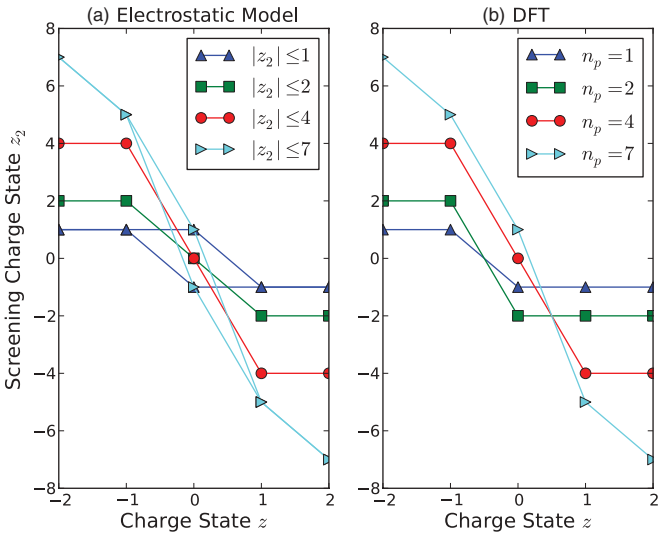


FIG. 10. (Color online) (a) Screening charge states that minimize the energy for the electrostatic model with different bounds to the screening charge $z_2$. (b) Corresponding DFT screening charge states for one, two, four, and seven ion pairs attached to the $Au_{39}$ cluster.

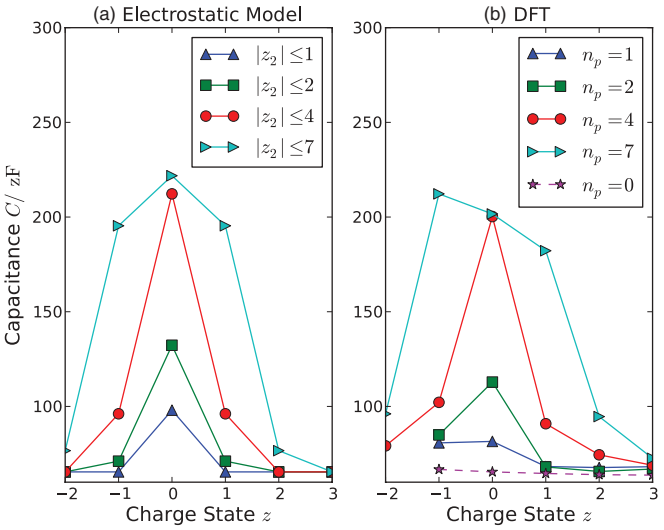


FIG. 11. (Color online) (a) Charge-dependent capacitance from the electrostatic model with different bounds to the screening charge state $z_2$. (b) Corresponding capacitance from DFT for the $Au_{39}$ cluster in contact without and with IL pairs.

which implies that a complete switch is predicted when going from $z = -1$ to $+1$. In the case of $n_p = 7$ still $z_2 = \mp 5$ is minimal at $z = \pm 1$ and all pairs' directions are switched for $z = \pm 2$.

Similar to EM, the minimizing configurations in DFT are separated by more than thermal energy in almost all cases. Exceptions are $n_p = 2, z = 0$, where $z_2 = 0, -2$ and $n_p = 7, z = -1$, where $z_2 = 3,5$ are nearly isoenergetic. The only difference to the EM is the stronger preference of negative ions near the neutral cluster for $n_p = 1$ and 2 that can be explained by the strong gold-anion binding. This trend does not persist for increasing $n_p$, however, as $z_2 = 0$ is preferred for four pairs and $z_2 = 1$ is 0.06 eV lower than $z_2 = -1$ for seven pairs and a neutral cluster.

Using the $E_{\min}(n_p,z)$, we can obtain the charge-dependent capacitance according to Eq. (5). The result is shown in Fig. 11. The EM predicts a distinct peak of the capacitance around charge state $z = 0$ independent of $n_p$ in agreement with the experimental observation.[18] The width of the peak increases with growing number of freely orientable ion pairs next to the cluster and is narrowed by the effect of overscreening ($|z_2| > |z|$). For seven pairs that did not completely switch the pair orientations for a single cluster charge, the capacitance peak forms shoulders. The appearance of the peak at $z = 0$ can be understood as follows. Fixing the charge state $z$, Eq. (11) takes its minimum at

$$z_2 = -\frac{z}{\alpha}, \tag{13}$$

which results in an overscreening effect for $0 < \alpha \leqslant 1$. Evaluating Eq. (11) at the minimum configuration yields an increased capacitance

$$C_{\mathrm{inc}} = \frac{C_1}{1 - \frac{C_1}{\alpha C_{23}}}. \tag{14}$$

The requirement $|z_2| \leqslant n_p$ results in a rectangular shape of the overall capacitance

$$C(z) = \frac{e^2}{\frac{\partial^2 E_{\min}}{\partial z^2}(z)} = \begin{cases} C_{\text{inc}} & \text{if } |z| \leqslant \alpha\, n_p, \\ C_1 & \text{if } |z| \geqslant \alpha\, n_p, \end{cases} \tag{15}$$

where $z$ is a real number. Quantized charging requires $C(z)$ to be calculated according to Eq. (5), which results in a peaklike shape instead of the rectangular shape of Eq. (15) for low bounds to the screening charge $z_2$. We note that, allowing a different bound for $z_2$ in the positive and negative regions, $z_2^- \leqslant z_2 \leqslant z_2^+$ leads to a shift of the negative wing to the left for $z_2^+ > n_p$ and to a shift of the positive wing to the right for $-z_2^- > n_p$, similar to the behavior found by Kornyshev[64] in the case of a planar double-layer capacitance for asymmetric maximal anion and cation concentrations.

As for the minimal $z_2$, the DFT results show very similar behavior of the capacitance both in the peak form as well as in the relative height of the peak. There is only a slight asymmetry due to the nonequivalence of cation and anion. Therefore, we note that the simple EM already captures the key feature of an increased capacitance near charge state $z = 0$ observed in our DFT calculations and the voltammetry study.[18]

The choice of the parameter $n_p$ corresponds to the question of how many freely orientable ion pairs are in contact with the cluster. A crude estimation can be made from the molar volume of the bulk ionic liquid and the surface area of the cluster. In our example, the first shell of ions is located at $r_2 \approx 9.6$ Å, which corresponds to an area of 1160 Å$^2$. The molar volume of $BMImBF_4$ is $1.88 \times 10^{-4}$ m$^3$ mol$^{-1}$ at 25 °C (Ref. 79) which gives an average area of 46 Å$^2$ per ion and suggests about 25 ion pairs could be attached to the cluster geometrically. Using $n_p = 25$ in the EM would lead to a plateaulike shape of $C(z)$ with constant capacitance in the considered charge range. The absence of a plateau in the experiment suggests that the number of rotatable pairs might be reduced.

## VI. CONCLUSIONS

In conclusion, we have analyzed the charging properties of gold clusters in different environments. There are two main influences visible for naked and monolayer protected clusters. First, the variation of the size of the electron cloud gives a slightly rising capacitance with increasing number of electrons. Second, shell-closing effects can strongly influence the charge-dependent capacitance leading to sudden "jumps" of this quantity.

The situation is different for clusters in a soft protecting and polarizable environment as exemplified by the situation in ILs. Here, the protecting IL layer can change its charge distribution through rearrangements of the ions. This leads to a strong enhancement of the capacitance for the neutral cluster that can be understood in a classical electrostatic model.

Cluster charging experiments such as cyclic voltammetry have to be performed in solution where the solvents dielectric constant $\epsilon$ largely influences the observed capacitance. The solvent effect can be approximately incorporated to the gas-phase results by scaling the calculated capacitance with $\epsilon$ which brings the values into good agreement to experiment.[18]

We finally note that our approach is not fully adiabatic as the clusters are only allowed to perform local relaxations when the cluster charge is changed. In particular, for small gold clusters it is known that there can be different ground-state structures depending on the cluster charge.[80] As a consequence, the cluster size where the transition for flat to three-dimensional structures happens depends on the charge.[81] Similar effects have been reported also for other metals.[82] A full study of the global minima at each charge state is unfortunately out of scope of this work. The change in the structure motive for different charges can be expected to be most severe for very small clusters, however. Whether a structural transition happens or not in the process of charging depends crucially on the barriers between the different structure motives,[83] the temperature, and the charging time involved in a possible experiment or technical realization.

## ACKNOWLEDGMENTS

M.W. wants to thank H. Häkkinen and M. Manninen for stimulating discussions about charging of clusters. We gratefully thank FZ Jülich, RZ Karlsruhe, and the bwGRiD project[84] for the computational resources.

[1] L. S. Ott and R. G. Finke, Coord. Chem. Rev. **251**, 1075 (2007).
[2] M. Walter and H. Häkkinen, Phys. Chem. Chem. Phys. **8**, 5407 (2006).
[3] B. Yoon, P. Koskinen, B. Huber, O. Kostko, B. von Issendorff, H. Häkkinen, M. Moseler, and U. Landman, Chem. Phys. Chem. **8**, 157 (2007).
[4] M. Moseler, M. Walter, B. Yoon, U. Landman, V. Habibpour, C. Harding, S. Kunz, and U. Heiz, J. Am. Chem. Soc. **134**, 7690 (2012).
[5] M.-C. Daniel and D. Astruc, Chem. Rev. **104**, 293 (2004).
[6] R. M. Crooks, M. Zhao, L. Sun, V. Chechik, and L. K. Yeung, Accounts Chem. Res. **34**, 181 (2001).
[7] C. Mirkin, R. Letsinger, R. Mucic, and J. Storhoff, Nature (London) **382**, 607 (1996).
[8] J. Dupont and J. D. Scholten, Chem. Soc. Rev. **39**, 1780 (2010).
[9] M. Homberger and U. Simon, Philos. Trans. R. Soc., A **368**, 1405 (2010).
[10] Y. Pei and X. C. Zeng, Nanoscale **4**, 4054 (2012).
[11] M. Walter, J. Akola, O. Lopez-Acevedo, P. D. Jadzinsky, G. Calero, C. J. Ackerson, R. L. Whetten, H. Grönbeck, and H. Häkkinen, Proc. Natl. Acad. Sci. USA **105**, 9157 (2008).
[12] H. Häkkinen, Chem. Soc. Rev. **37**, 1847 (2008).
[13] D. Jiang, Chem. Eur. J. **17**, 12289 (2011).
[14] H. Häkkinen, Nat. Chem. **4**, 443 (2012).
[15] B. M. Quinn, P. Liljeroth, V. Ruiz, T. Laaksonen, and K. Kontturi, J. Am. Chem. Soc. **125**, 6644 (2003).
[16] S. F. Mertens, K. Blech, A. S. Sologubenko, J. Mayer, U. Simon, and T. Wandlowski, Electrochim. Acta **54**, 5006 (2009).

[17]V. Garcia-Morales and S. Mafé, J. Phys. Chem. C **111**, 7242 (2007).
[18]S. F. L. Mertens, C. Vollmer, A. Held, M. H. Aguirre, M. Walter, C. Janiak, and T. Wandlowski, Angew. Chem. Int. Ed. **50**, 9735 (2011).
[19]F. Weigend, F. Evers, and J. Weissmüller, Small **2**, 1497 (2006).
[20]Q. Wang, Q. Sun, Z. J. Yu, M. Sakurai, and Y. Kawazoe, Scr. Mater. **44**, 1959 (2001).
[21]P. Hohenberg and W. Kohn, Phys. Rev. **136**, B864 (1964).
[22]W. Kohn and L. J. Sham, Phys. Rev. **140**, A1133 (1965).
[23]P. E. Blöchl, Phys. Rev. B **50**, 17953 (1994).
[24]J. J. Mortensen, L. B. Hansen, and K. W. Jacobsen, Phys. Rev. B **71**, 035109 (2005).
[25]J. Enkovaara, C. Rostgaard, J. J. Mortensen, J. Chen, M. Dułak, L. Ferrighi, J. Gavnholt, C. Glinsvad, V. Haikola, H. A. Hansen, H. H. Kristoffersen, M. Kuisma, A. H. Larsen, L. Lehtovaara, M. Ljungberg, O. Lopez-Acevedo, P. G. Moses, J. Ojanen, T. Olsen, V. Petzold, N. A. Romero, J. Stausholm-Møller, M. Strange, G. A. Tritsaris, M. Vanin, M. Walter, B. Hammer, H. Häkkinen, G. K. H. Madsen, R. M. Nieminen, J. K. Nørskov, M. Puska, T. T. Rantala, J. Schiøtz, K. S. Thygesen, and K. W. Jacobsen, J. Phys.: Condens. Matter **22**, 253202 (2010).
[26]J. P. Perdew, K. Burke, and M. Ernzerhof, Phys. Rev. Lett. **77**, 3865 (1996).
[27]J. Tao, J. P. Perdew, V. N. Staroverov, and G. E. Scuseria, Phys. Rev. Lett. **91**, 146401 (2003).
[28]E. Redel, M. Walter, R. Thomann, C. Vollmer, L. Hussein, H. Scherer, M. Krüger, and C. Janiak, Chem. Eur. J. **15**, 10047 (2009).
[29]E. Redel, M. Walter, R. Thomann, L. Hussein, M. Krüger, and C. Janiak, Chem. Commun. **46**, 1159 (2010).
[30]J. R. Reimers and N. S. Hush, J. Phys. Chem. B **105**, 8979 (2001).
[31]P. Senet and M. Hou, Nanostruct. Mater. **12**, 361 (1999).
[32]R. J. C. Batista, M. S. C. Mazzoni, and H. Chacham, Nanotechnology **21**, 065705 (2010).
[33]R. G. Parr and W. Yang, *Density-Functional Theory of Atoms and Molecules* (Oxford University Press, Oxford, 1989).
[34]R. G. Pearson, Proc. Natl. Acad. Sci. USA **83**, 8440 (1986).
[35]J. P. Perdew, Phys. Rev. B **37**, 6175 (1988).
[36]J. P. Perdew, M. Brajczewska, and C. Fiolhais, Solid State Commun. **88**, 795 (1993).
[37]M. Seidl, J. P. Perdew, M. Brajczewska, and C. Fiolhais, J. Chem. Phys. **108**, 8182 (1998).
[38]J. Li, X. Li, H.-J. Zhai, and L.-S. Wang, Science **299**, 864 (2003).
[39]P. Gruene, D. M. Rayner, B. Redlich, A. F. G. van der Meer, J. T. Lyon, G. Meijer, and A. Fielicke, Science **321**, 674 (2008).
[40]P. D. Jadzinsky, G. Calero, C. J. Ackerson, D. A. Bushnell, and R. D. Kornberg, Science **318**, 430 (2007).
[41]B. Assadollahzadeh and P. Schwerdtfeger, J. Chem. Phys. **131**, 064306 (2009).
[42]S. Lias, R. Levin, and S. Kafafi, in *NIST Chemistry WebBook, NIST Standard Reference Database*, 69, edited by P. Linstrom and W. Mallard (National Institute of Standards and Technology, Gaithersburg, MD, 2012).
[43]J. Bartmess, in *NIST Chemistry WebBook, NIST Standard Reference Database*, 69, edited by P. Linstrom and W. Mallard (National Institute of Standards and Technology, Gaithersburg, MD, 2012).
[44]C. Jackschath, I. Rabin, and W. Schulze, Ber. Bunsenges. Phys. Chem. **96**, 1200 (1992).
[45]W. A. Saunders, Phys. Rev. Lett. **64**, 3046 (1990).
[46]U. Näher, S.Bjørnholm, S. Frauendorf, F. Garcias, and C. Guet, Phys. Rep. **285**, 245 (1997).
[47]J. Bowlan, A. Liang, and W. A. de Heer, Phys. Rev. Lett. **106**, 043401 (2011).
[48]P. Ball, Nat. Mater. **10**, 175 (2011).
[49]J. P. Perdew and Y. Wang, Phys. Rev. B **45**, 13244 (1992).
[50]We consider 11 valence electrons per gold atom in the calculation. The 10 *d* electrons per atom occupy 5 states resulting in 195 *d* derived states in the $Au_{39}$ cluster. The states around Fermi energy are derived from atomic *s* states while the filled *d*-derived states are deeper in energy (Refs. 2 and 3). We therefore obtain the *s* valence count by subtracting 195 states from the total valence count.
[51]W. A. de Heer, Rev. Mod. Phys. **65**, 611 (1993).
[52]B. K. Teo, X. Shi, and H. Zhang, J. Am. Chem. Soc. **114**, 2743 (1992).
[53]H. Häkkinen, M. Walter, and H. Grönbeck, J. Phys. Chem. B **110**, 9927 (2006).
[54]D.-e. Jiang and M. Walter, Phys. Rev. B **84**, 193402 (2011).
[55]M. Heaven, A. Dass, P. White, K. Holt, and R. Murray, J. Am. Chem. Soc. **130**, 3754 (2008).
[56]M. Zhu, C. M. Aikens, F. J. Hollander, G. C. Schatz, and R. Jin, J. Am. Chem. Soc. **130**, 5883 (2008).
[57]H. Qian, W. T. Eckenhoff, Y. Zhu, T. Pintauer, and R. Jin, J. Am. Chem. Soc. **132**, 8280 (2010).
[58]J. Akola, M. Walter, R. Whetten, H. Häkkinen, and H. Grönbeck, J. Am. Chem. Soc. **130**, 3756 (2008).
[59]Y. Pei, Y. Gao, and X. C. Zeng, J. Am. Chem. Soc. **130**, 7830 (2008).
[60]O. Lopez-Acevedo, H. Tsunoyama, T. Tsukuda, H. Häkkinen, and C. M. Aikens, J. Am. Chem. Soc. **132**, 8210 (2010).
[61]D. M. P. Mingos, J. Chem. Soc., Dalton Trans., 561 (1996).
[62]M. Walter, M. Moseler, R. L. Whetten, and H. Häkkinen, Chem. Science **2**, 1583 (2011).
[63]T. Laaksonen, V. Ruiz, P. Liljeroth, and B. M. Quinn, Chem. Soc. Rev. **37**, 1836 (2008).
[64]A. A. Kornyshev, J. Phys. Chem. B **111**, 5545 (2007).
[65]M. V. Fedorov and A. A. Kornyshev, Electrochim. Acta **53**, 6835 (2008).
[66]D. Jiang, D. Meng, and J. Wu, Chem. Phys. Lett. **504**, 153 (2011).
[67]R. Hayes, N. Borisenko, M. K. Tam, P. C. Howlett, F. Endres, and R. Atkin, J. Phys. Chem. C **115**, 6855 (2011).
[68]D. A. Turton, A. S. Johannes Hunger, G. Hefter, A. Thoman, M. Walther, R. Buchner, and K. Wynne, J. Am. Chem. Soc. **131**, 11140 (2009).
[69]B. Kirchner, Top. Curr. Chem. **290**, 213 (2009).
[70]1-N-butyl-3-methylimidazolium ($BMIm^+$) is also named as $[C_4mim]^+$ or $C_4C_1im^+$ in the literature.
[71]P. A. Hunt, I. R. Gould, and B. Kirchner, Australian J. Chem. **60**, 9 (2007).
[72]S. Grimme, W. Hujoa, and B. Kirchner, Phys. Chem. Chem. Phys. **14**, 4875 (2012).
[73]D. C. Langreth, B. I. Lundqvist, S. D. Chakarova-Käck, V. R. Cooper, M. Dion, P. Hyldgaard, A. Kelkkanen, J. Kleis, L. Kong, S. Li, P. G. Moses, E. Murray, A. Puzder, H. Rydberg, E. Schröder, and T. Thonhauser, J. Phys.: Condens. Matter **21**, 084203 (2009).
[74]A. Tkatchenko and M. Scheffler, Phys. Rev. Lett. **102**, 073005 (2009).
[75]The electric dipole moment of a $BF_4$ BMIm pair calculated from the electron density is 3.00 eÅ and therefore clearly smaller than the simple geometric dipole.
[76]S. A. Katsyuba, E. E. Zvereva, N. Yan, X. Yuan, Y. Kou, and P. J. Dyson, Chem. Phys. Chem. **13**, 1781 (2012).
[77]Y. Levin, Rep. Prog. Phys. **65**, 1577 (2002).

[78]The positions of $BF_4^-$ and $BMIm^+$ are approximated by the position of the boron atom and the center of mass of the nitrogen atoms, respectively. The distance to the gold clusters surface is approximated by the distance to the nearest gold atom.

[79]J. N. Canongia Lopes, T. C. Cordeiro, J. M. S. S. Esperana, H. J. R. Guedes, S. Huq, L. P. N. Rebelo, and K. R. Seddon, J. Phys. Chem. B **109**, 3519 (2005).

[80]H. Häkkinen and U. Landman, Phys. Rev. B **62**, R2287 (2000).

[81]L. Ferrighi, B. Hammer, and G. K. H. Madsen, J. Am. Chem. Soc. **131**, 10605 (2009).

[82]S. Núñez, J. M. López, and A. Aguado, Nanoscale **4**, 6481 (2012).

[83]P. Koskinen, H. Häkkinen, B. Huber, B. von Issendorff, and M. Moseler, Phys. Rev. Lett. **98**, 015701 (2007).

[84]bwGRiD (http://www.bw-grid.de), member of the German D-Grid initiative, funded by the Ministry for Education and Research and the Ministry for Science, Research and Arts Baden-Wuerttemberg.